Near-infrared and optical broadband surface photometry of 86 face-on disk dominated galaxies

de Jong, R. S.

Published in:
Astronomy & astrophysics supplement series

DOI:
10.1051/aas:1996220

Publication date:
1996

ASTRONOMY & ASTROPHYSICS
SUPPLEMENT SERIES

SEPTEMBER **1996**, PAGE 557

Astron. Astrophys. Suppl. Ser. **118,** 557-573 (1996)

Near-infrared and optical broadband surface photometry of 86 face-on disk dominated galaxies.⋆,⋆⋆ II. A two-dimensional method to determine bulge and disk parameters

R.S. de Jong

Kapteyn Astronomical Institute, P.O. Box 800, NL-9700 AV Groningen, The Netherlands

Received May 19; accepted October 9, 1995

Abstract. — In this Paper I present a new two-dimensional decomposition technique, which models the surface photometry of a galaxy with an exponential light profile for both bulge and disk and, when necessary, with a Freeman bar. The new technique was tested for systematic errors on both artificial and real data and compared with widely used one-dimensional decomposition techniques, where the luminosity profile of the galaxy is used. The comparisons indicate that a decomposition of the two-dimensional image of the galaxy with an exponential light profile for both bulge and disk yields the most reproducible and representative bulge and disk parameters. An extensive error analysis was made to determine the reliability of the model parameters. If the model with an exponential bulge profile is a reasonable description of a galaxy, the maximum errors in the derived model parameters are of order 20%. The uncertainties in the model parameters will increase, if the exponential bulge function is replaced by other often used bulge functions as the de Vaucouleurs law. All decomposition methods were applied to the optical and near-infrared data set presented by de Jong & van der Kruit (1994), which comprises 86 galaxies in six passbands.

Key words: methods: data analysis — surveys — galaxies: fundamental parameters — galaxies: photometry — galaxies: spiral — galaxies: structure

1. Introduction

The light distribution of disk dominated galaxies is often decomposed into a bulge and a disk component which are assumed to be physically and dynamically distinct. The disk component is flat and governed by rotational dynamics. The spherical bulge component, though mainly rotationally supported against gravity, is dynamically a much hotter system than the disk. Whether this separation is real is hard to say; it is likely that a dynamical interplay exists between the different components in the dense inner regions of galaxies. Separating both components using only the surface photometry of a galaxy has been a long-standing problem.

When we assume that there are distinct components, the parameters describing the light distribution of these components are of fundamental importance. They reveal the common properties among galaxies and especially in combination with dynamics and (chemical) content they are tracers of galaxy formation and evolution. Two well-known relations with fundamental component parameters are the constancy of central surface brightness among disks of spiral galaxies (Freeman 1970) and the link between bulge-to-disk (B/D) ratio and the Hubble classification sequence.

Many different decomposition techniques can be found in the literature (for reviews see e.g. Simien 1989; Capaccioli & Caon 1992). For most of the methods one postulates some mathematical functions describing the shape of the different components, after which the sum of the components functions is fitted to the observed light distribution. Decomposition techniques differ in both the

Send offprint requests to: R.S. de Jong, University of Durham, Dept. of Physics, South Road, Durham, DH1 3LE, UK, e-mail: R.S.deJong@Durham.ac.uk

⋆Based on observations with the Jacobus Kapteyn Telescope operated by the Royal Greenwich Observatory at the Observatorio del Roque de los Muchachos of the Instituto de Astrofísica de Canarias with financial support from the PPARC (UK) and NWO (NL) and with the UK Infrared Telescope at Mauna Kea operated by the Royal Observatory Edinburgh with financial support of the PPARC

⋆⋆The tables are also available in electronic form via anonymous ftp 130.79.128.5

assumed mathematical functions as well as in the applied fitting algorithms.

The most frequently used function describing the radial surface brightness profile of the disks of spiral galaxies is the exponential function

$$\Sigma_{\rm disk}(r) = \Sigma_0 {\rm e}^{-r/h} \quad (1)$$

or in magnitudes

$$\mu_{\rm disk}(r) = \mu_0 + 1.086 r/h \quad (2)$$

with μ_0 (Σ_0) being the central surface brightness (luminosity) and h the scalelength of the exponential disk. The exponential function is not always a good description of the disk light profile. After the bulge light is subtracted from the luminosity profile, the disk profiles of spiral galaxies sometimes show a deficit of light in their inner regions (Type II profiles, Freeman 1970). An improved disk model in the form of a modified exponential profile (Kormendy 1977) is therefore sometimes fitted to these Type II profiles. Furthermore, it should be noted that the exponential model profile might need a truncation. Especially in edge-on galaxies a sudden decrease in light has often been detected at large radii (van der Kruit 1979).

Compared to the disk profile there is less consensus on the mathematical function to be used for the bulge light profile, because only the central bright part of the bulge can be seen in most spiral galaxies. Away from the center the bulge light is hidden underneath the disk light for a face-on galaxy and therefore only the central region can be used to determine the shape of the bulge luminosity profile. The most widely used bulge function is the $r^{1/4}$ law (de Vaucouleurs 1948). This function generally gives a good description of the light distribution of elliptical galaxies and was first used for spiral bulges, in combination with an exponential disk, by de Vaucouleurs (1959). The motivation to use the same fitting function for elliptical galaxies and bulges is an assumed evolutionary or at least structural sequence from ellipticals to spirals (or vice versa). The shape of elliptical luminosity profiles are not completely undisputed and therefore all light profile functions proposed for ellipticals (e.g. Hubble profiles (1930), King profiles (1966), Jaffe profiles (1983) or generalized exponentials (Caon et al. 1993; D'Onofrio et al. 1994)) could in principle also be used for bulges. Kormendy (1977) showed that the parameters of the Hubble, King and de Vaucouleurs profiles describe the same physical quantities for ellipticals.

One should be careful in making the link between elliptical galaxies and bulges of spiral galaxies. The presence of the disk will influence the dynamics of the bulge, especially for late-type systems with a low B/D ratio. Bulges are for a considerable fraction rotationally supported against gravity and not largely pressure supported as are elliptical galaxies (Kormendy & Illingworth 1982; Kormendy 1993 and references therein). Also deviations from the $r^{1/4}$ law have been observed in bulges of edge-on spirals (Frankston & Schild 1976; Kormendy & Bruzual 1978; Burstein 1979; Jensen & Thuan 1979; Shaw & Gilmore 1989; Wainscoat et al. 1989, Kent et al. 1991). These deviations have motivated Frankston & Schild (1976), Kent et al. (1991) and Andredakis & Sanders (1994) to propose exponential functions for bulge profiles.

Decomposition techniques using the change in ellipticities and position angles of the isophotes (Kent 1986) have the advantage that they do not have to assume fitting functions. They can work perfectly well assuming that spiral galaxies are only made of ellipsoids/tori with changing inclinations. But as real galaxies contain bars, spiral arms and dust lanes these methods will have systematic errors. They only work reasonably well on systems with a high inclination, where the difference in the flattening of the disk and the bulge component is easily measurable.

Decompositions using all the pixels in the full image instead of the one-dimensional (1D) profile of galaxies take little precedence in the literature. The main reason for this being the lack of computer power and an additional reason being the difficulties due to the presence of bars and spiral arms. These are conveniently averaged out in 1D profiles. Two-dimensional (2D) fitting techniques have been applied before on small samples of elliptical galaxies and S0's (Capaccioli et al. 1987; Simien & Michard 1990; Scorza & Bender 1990), but only once before on a large set of spiral galaxies (Byun 1992). Two-dimensional fitting has the same advantage as Kent's method (Kent 1986) in that one uses the difference in projected ellipticities of disk and bulge. The sample used here was selected to be face-on and the differences in ellipticities are expected to be small. Still the 2D fitting technique is applied, because it has the advantage to 1D fitting that non-axisymmetric components can be fitted as well. The method applied here has a non-axisymmetric component in the form of a bar, which will improve the fitting results of the disk and especially the bulge component.

The bulge and disk parameters determined by the 2D method will be used in subsequent papers to determine the relationships among the structural parameters of galaxies. To assess the reliability of these relationships a thorough error analysis is needed. In this Paper I will discuss several sources of error, most notably the effects of 1D versus 2D fitting, the uncertainty in the shape of disk and bulge profiles, influences of measurement errors and the effect of different radial weighting functions.

The structure of this paper is as follows. The observational data are briefly described in Sect. 2. The 2D fitting technique is explained and tested in Sect. 3. In Sect. 4 the 2D fitting technique is compared with several 1D fitting techniques. The results of all tests and comparisons are used in the error discussion in Sect. 5. The main conclusions are summarized in Sect. 6.

2. The data

In order to examine the parameters describing the global structure of spiral galaxies, 86 systems were observed in the B, V, R, I, H and K passbands. A full description of the observations and data reduction can be found in de Jong & van der Kruit (1994, hereafter Paper I), which will be repeated only very briefly here. The galaxies in this statistically complete sample of undisturbed spirals were selected from the UGC (Nilson 1973) to have red diameters of at least two minutes of arc and minor over major axis ratios larger than 0.625. The galaxies were imaged along the major axis with the 1m Jacobus Kapteyn Telescope on La Palma in the B, V, R and I passbands and with the United Kingdom Infra-Red Telescope on Hawaii in the H and K passbands. Standard reduction techniques (bias subtraction, flatfielding by twilight flatfields, calibration by standard stars) were used to produce calibrated images. The sky brightness was determined outside the galaxy in areas free of stars and its uncertainty (mainly due to flatfield limitations) constitutes one of the main sources of error in the derived parameters.

The ellipticity and position angle (PA) of each galaxy were determined at an outer isophote. The radial surface brightness profiles were determined by calculating the average surface brightness on elliptical rings of increasing radii using the determined ellipticity and PA. Internal and external comparisons showed that the derived parameters were well within the estimated errors. These estimated errors are included in the analysis discussed here.

3. Two-dimensional decomposition

In this section the 2D fitting technique is described. The motivation for using the 2D method was the large number of galaxies in the sample with a pronounced bar, which cannot be fitted in 1D models. The different model components are described and the fitting procedure followed is explained in some detail. The fitting technique was tested on both artificial and real data and is shown to be very accurate in most realistic cases. Finally, the results for the data set are presented for the B and the K passband.

3.1. *Advantages of two-dimensional fitting*

In the literature one encounters mainly the use of 1D profiles to perform bulge/disk decompositions. The extraction of the profiles improves the signal-to-noise, but the non-axisymmetric information present in the image is lost. Bars can have considerable influence on profiles (see for example in Paper I UGC 89, UGC 6536, UGC 7523, UGC 7594, UGC 8865 and UGC 12776). These features will make 1D bulge/disk decompositions incorrect, even if the fits seem correct and the χ^2 values are low. One-dimensional models fitted to azimuthally averaged profiles can never include a bar.

A considerable fraction of spiral galaxies are barred. Of the 86 galaxies of our sample only 13 were classified as non-barred according the RC3 (de Vaucouleurs et al. 1991) and 12 galaxies had no bar classification. Therefore fitting bars is desirable, especially if one considers that bars are more pronounced in the near-IR (Block & Wainscoat 1991). This can only be done by fitting the full 2D images. An additional advantage of the 2D technique is that the difference in the flattening of the bulge and the disk is also used for the few systems in the sample with higher inclination.

The technique of fitting models to the full images of spiral galaxies has little precedence in the literature. Shaw & Gilmore (1989) fitted 2D models to two edge-on galaxies, the configuration where disk and bulge are the most distinct. Byun (1992) used a data set of 1355 I passband images of galaxies with inclinations larger than $i > 40^{\rm o}$. From tests on artificial data, Byun showed that the 2D method was better in reproducing the model input parameters than the 1D method. Neither Shaw & Gilmore nor Byun included a bar in their fits.

3.2. *The model components*

The 2D model consists of two or three components. First of all, a spherically symmetrical bulge with an exponential radial light distribution. The use of an exponential bulge profile instead of the more widely used $r^{1/4}$ law profile (de Vaucouleurs 1948) was motivated by the work of Andredakis & Sanders (1994) and the work presented in Sect. 4. Bulge parameters are normally expressed in effective parameters which translates the exponential law into

$$\Sigma_{\rm bulge}(r) = \Sigma_{\rm e} {\rm e}^{-1.679(r/r_{\rm e}-1)}, \qquad (3)$$

where the effective radius ($r_{\rm e}$) encloses half the total luminosity and $\Sigma_{\rm e}$ is the surface brightness ($\mu_{\rm e}$ in mag) at this radius. In the cartesian coordinate system of the CCD image r should be read as $\sqrt{x^2+y^2}$, with the center of the coordinate system at the galaxy center.

The second component, the disk, is described by Eq. (1) and has the usual two free parameters of an exponential light distribution (Σ_0 and h). Due to inclination though, the disk has two additional parameters: minor over major axis ratio (b/a) and position angle (PA) and r should be read as $\sqrt{([x\cos({\rm PA}) + y\sin({\rm PA})]\frac{b}{a})^2 + (-x\sin({\rm PA}) + y\cos({\rm PA}))^2}$ in the carthesian coordinate system. Fitting with b/a and PA as free parameters was tried, but it turned out that the fitting routine often adjusted the b/a and PA in such a way that spiral arms and bars were modeled, instead of the global disk properties. Therefore I decided to keep b/a and PA fixed to the values determined at the outer isophotes (the same values that were used for extracting the radial profiles).

Table 1. The relative errors between input artificial image parameters and fitted bulge and disk parameters determined using the 2D fit method. Tabulated are the results for the standard artificial galaxy as described in the text, as well as the effect of a wrong estimate of one of the parameters which were normally kept fixed to the observed values while fitting the model (see notes). Relative errors are listed, with $\Delta\mu_0 = \mu_{0,\rm art} - \mu_{0,\rm fit}$ and $\Delta\mu_{\rm e} = \mu_{\rm e,art} - \mu_{\rm e,fit}$ in mag arcsec^{-2}, $\Delta h = 2(h_{\rm art} - h_{\rm fit})/(h_{\rm art} + h_{\rm fit})$ and $\Delta r_{\rm e} = 2(r_{\rm e,art} - r_{\rm e,fit})/(r_{\rm e,art} + r_{\rm e,fit})$ dimensionless

$\mu_{\rm e,art}$	$r_{\rm e,art}$	$\Delta\mu_0$									Δh								
		stand.	seeing	seeing error		sky error		b/a error		PA	stand.	seeing	seeing error		sky error		b/a error		PA
			2.5″	−0.1″	+0.1″	+1%	−1%	−0.1	+0.1	+20°		2.5″	−0.1″	+0.1″	+1%	−1%	−0.1	+0.1	+20°
(1)	(2)	(3)	(4)	(5)	(6)	(7)	(8)	(9)	(10)	(11)									
17	4.0	-0.012	-0.042	-0.034	0.011	0.088	-0.090	0.034	-0.056	-0.051	-0.005	-0.016	-0.013	0.004	0.083	-0.083	0.094	-0.093	-0.023
18	4.0	-0.005	-0.019	-0.015	0.004	0.094	-0.084	0.041	-0.050	-0.044	-0.001	-0.007	-0.005	0.002	0.086	-0.080	0.096	-0.091	-0.021
19	4.0	-0.002	-0.009	-0.006	0.001	0.096	-0.082	0.043	-0.048	-0.042	-0.001	-0.004	-0.002	0.001	0.086	-0.079	0.097	-0.090	-0.020
20	4.0	-0.002	-0.005	-0.003	0.000	0.095	-0.082	0.043	-0.049	-0.042	-0.000	-0.002	-0.001	0.000	0.086	-0.080	0.097	-0.090	-0.020
21	4.0	-0.001	-0.003	-0.002	-0.001	0.091	-0.085	0.041	-0.052	-0.043	-0.000	-0.001	-0.000	-0.000	0.084	-0.081	0.096	-0.092	-0.021
17	3.0	-0.013	-0.032	-0.029	0.004	0.070	-0.078	0.021	-0.046	-0.043	-0.005	-0.013	-0.011	0.002	0.077	-0.078	0.089	-0.089	-0.020
18	3.0	-0.005	-0.015	-0.013	0.001	0.077	-0.073	0.028	-0.040	-0.036	-0.002	-0.006	-0.005	0.001	0.079	-0.076	0.091	-0.087	-0.018
19	3.0	-0.003	-0.008	-0.006	-0.001	0.079	-0.071	0.029	-0.038	-0.034	-0.001	-0.003	-0.002	0.000	0.080	-0.075	0.092	-0.086	-0.017
20	3.0	-0.002	-0.004	-0.003	-0.001	0.079	-0.071	0.030	-0.038	-0.033	-0.001	-0.002	-0.001	-0.000	0.080	-0.075	0.092	-0.086	-0.017
21	3.0	-0.002	-0.003	-0.002	-0.002	0.077	-0.073	0.030	-0.039	-0.034	-0.000	-0.001	-0.001	-0.000	0.079	-0.076	0.092	-0.086	-0.017
17	2.0	-0.013	-0.006	-0.023	-0.001	0.058	-0.070	0.013	-0.039	-0.037	-0.005	-0.003	-0.009	-0.000	0.072	-0.075	0.086	-0.086	-0.018
18	2.0	-0.006	-0.004	-0.011	-0.002	0.064	-0.064	0.019	-0.034	-0.031	-0.002	-0.001	-0.004	-0.000	0.074	-0.072	0.088	-0.084	-0.016
19	2.0	-0.004	-0.003	-0.005	-0.002	0.066	-0.061	0.022	-0.032	-0.029	-0.001	-0.001	-0.002	-0.000	0.075	-0.071	0.089	-0.083	-0.015
20	2.0	-0.003	-0.003	-0.003	-0.002	0.066	-0.061	0.022	-0.031	-0.028	-0.001	-0.001	-0.001	-0.000	0.075	-0.071	0.089	-0.083	-0.015
21	2.0	-0.002	-0.003	-0.003	-0.002	0.065	-0.063	0.022	-0.031	-0.028	-0.001	-0.001	-0.001	-0.001	0.074	-0.072	0.089	-0.083	-0.015
17	1.0	0.001	0.016	-0.008	0.009	0.063	-0.050	0.023	-0.024	-0.021	0.001	0.007	-0.003	0.004	0.074	-0.066	0.089	-0.080	-0.012
18	1.0	-0.001	0.004	-0.005	0.002	0.061	-0.053	0.020	-0.026	-0.023	-0.000	0.002	-0.002	0.001	0.073	-0.067	0.088	-0.081	-0.013
19	1.0	-0.002	-0.001	-0.004	-0.001	0.059	-0.054	0.019	-0.027	-0.024	-0.001	-0.000	-0.001	-0.000	0.072	-0.068	0.088	-0.081	-0.013
20	1.0	-0.003	-0.003	-0.003	-0.002	0.058	-0.055	0.018	-0.027	-0.025	-0.001	-0.001	-0.001	-0.001	0.072	-0.068	0.088	-0.081	-0.013
21	1.0	-0.003	-0.004	-0.003	-0.003	0.057	-0.056	0.021	-0.028	-0.025	-0.001	-0.001	-0.001	-0.001	0.071	-0.069	0.089	-0.082	-0.013
17	0.5	0.002	-0.001	0.000	0.003	0.061	-0.047	0.023	-0.021	-0.018	0.001	-0.000	0.001	0.001	0.073	-0.065	0.089	-0.079	-0.010
18	0.5	-0.001	-0.003	-0.002	-0.001	0.057	-0.050	0.019	-0.025	-0.022	-0.000	-0.001	-0.000	-0.000	0.071	-0.066	0.088	-0.080	-0.012
19	0.5	-0.003	-0.004	-0.003	-0.003	0.056	-0.051	0.017	-0.026	-0.023	-0.001	-0.002	-0.001	-0.001	0.071	-0.067	0.087	-0.081	-0.013
20	0.5	-0.003	-0.005	-0.003	-0.003	0.055	-0.053	0.017	-0.027	-0.024	-0.001	-0.002	-0.001	-0.001	0.071	-0.068	0.087	-0.081	-0.013
21	0.5	-0.003	-0.005	-0.003	-0.003	0.055	-0.156	0.017	-0.027	-0.264	-0.001	-0.002	-0.001	-0.001	0.071	-0.104	0.087	-0.081	0.017

$\mu_{\rm e,art}$	$r_{\rm e,art}$	$\Delta\mu_{\rm e}$									$\Delta r_{\rm e}$								
		stand.	seeing	seeing error		sky error		b/a error		PA	stand.	seeing	seeing error		sky error		b/a error		PA
			2.5″	−0.1″	+0.1″	+1%	−1%	−0.1	+0.1	+20°		2.5″	−0.1″	+0.1″	+1%	−1%	−0.1	+0.1	+20°
17	4.0	-0.007	-0.021	-0.019	0.004	-0.007	-0.008	-0.006	-0.009	-0.008	-0.010	-0.029	-0.016	-0.004	-0.006	-0.013	-0.007	-0.012	-0.012
18	4.0	-0.007	-0.022	-0.019	0.004	-0.005	-0.009	-0.004	-0.010	-0.010	-0.010	-0.029	-0.016	-0.003	-0.000	-0.017	-0.003	-0.016	-0.014
19	4.0	-0.008	-0.024	-0.019	0.004	-0.002	-0.012	0.001	-0.015	-0.013	-0.009	-0.029	-0.015	-0.003	0.014	-0.027	0.008	-0.025	-0.021
20	4.0	-0.008	-0.029	-0.019	0.003	0.005	-0.021	0.013	-0.029	-0.023	-0.007	-0.029	-0.014	-0.001	0.049	-0.054	0.033	-0.049	-0.038
21	4.0	-0.010	-0.041	-0.021	0.002	0.021	-0.046	0.037	-0.073	-0.050	-0.004	-0.029	-0.011	0.002	0.132	-0.129	0.090	-0.121	-0.087
17	3.0	-0.011	-0.046	-0.028	0.006	-0.010	-0.012	-0.010	-0.012	-0.012	-0.017	-0.050	-0.026	-0.009	-0.014	-0.020	-0.015	-0.019	-0.019
18	3.0	-0.011	-0.046	-0.028	0.007	-0.007	-0.014	-0.007	-0.014	-0.013	-0.017	-0.050	-0.026	-0.008	-0.007	-0.025	-0.011	-0.022	-0.021
19	3.0	-0.010	-0.048	-0.027	0.007	0.000	-0.019	-0.001	-0.019	-0.017	-0.016	-0.050	-0.024	-0.007	0.010	-0.036	-0.001	-0.030	-0.027
20	3.0	-0.010	-0.053	-0.027	0.008	0.014	-0.033	0.012	-0.033	-0.027	-0.014	-0.048	-0.022	-0.005	0.048	-0.067	0.023	-0.051	-0.043
21	3.0	-0.010	-0.068	-0.028	0.008	0.045	-0.078	0.041	-0.078	-0.057	-0.009	-0.046	-0.018	0.000	0.141	-0.155	0.077	-0.115	-0.088
17	2.0	-0.032	-0.105	-0.061	-0.003	-0.030	-0.035	-0.031	-0.034	-0.034	-0.039	-0.087	-0.054	-0.026	-0.034	-0.044	-0.038	-0.042	-0.042
18	2.0	-0.031	-0.105	-0.060	-0.001	-0.024	-0.037	-0.027	-0.035	-0.035	-0.039	-0.087	-0.053	-0.025	-0.026	-0.049	-0.033	-0.044	-0.044
19	2.0	-0.030	-0.105	-0.059	0.000	-0.012	-0.045	-0.020	-0.040	-0.038	-0.036	-0.083	-0.051	-0.022	-0.005	-0.062	-0.022	-0.051	-0.049
20	2.0	-0.027	-0.107	-0.057	0.004	0.015	-0.067	-0.002	-0.054	-0.048	-0.032	-0.077	-0.046	-0.017	0.043	-0.099	0.004	-0.070	-0.063
21	2.0	-0.020	-0.112	-0.052	0.012	0.077	-0.141	0.037	-0.099	-0.079	-0.021	-0.062	-0.038	-0.005	0.157	-0.208	0.062	-0.127	-0.104
17	1.0	-0.121	-0.115	-0.209	-0.022	-0.112	-0.130	-0.118	-0.125	-0.125	-0.096	-0.072	-0.144	-0.045	-0.086	-0.105	-0.093	-0.101	-0.100
18	1.0	-0.121	-0.106	-0.209	-0.022	-0.096	-0.142	-0.112	-0.131	-0.130	-0.096	-0.064	-0.142	-0.043	-0.070	-0.118	-0.086	-0.105	-0.104
19	1.0	-0.120	-0.086	-0.209	-0.021	-0.060	-0.172	-0.097	-0.146	-0.142	-0.095	-0.048	-0.142	-0.042	-0.032	-0.148	-0.072	-0.120	-0.116
20	1.0	-0.120	-0.042	-0.211	-0.019	0.023	-0.250	-0.064	-0.184	-0.172	-0.092	-0.009	-0.140	-0.038	0.058	-0.227	-0.035	-0.157	-0.144
21	1.0	-0.142	0.050	-0.215	-0.016	0.191	-0.501	1.107	-0.282	-0.243	-0.101	0.078	-0.135	-0.031	0.246	-0.469	0.717	-0.249	-0.213
17	0.5	0.001	0.115	-0.368	0.467	0.052	-0.041	0.018	-0.018	-0.014	-0.028	0.037	-0.214	0.198	0.010	-0.053	-0.014	-0.037	-0.037
18	0.5	-0.033	0.125	-0.390	0.417	0.087	-0.139	0.008	-0.082	-0.073	-0.043	0.047	-0.227	0.174	0.037	-0.115	-0.018	-0.075	-0.071
19	0.5	-0.111	0.145	-0.441	0.305	0.169	-0.372	-0.015	-0.229	-0.207	-0.084	0.073	-0.253	0.116	0.105	-0.262	-0.018	-0.163	-0.150
20	0.5	-0.270	0.175	-0.547	0.072	0.340	-0.894	-0.192	-0.536	-0.478	-0.167	0.121	-0.308	0.000	0.257	-0.613	-0.053	-0.357	-0.316
21	0.5	-0.529	0.192	-0.750	-0.304	1.016	-2.653	-0.479	-1.122	-2.505	-0.301	0.227	-0.408	-0.192	0.865	-1.851	-0.167	-0.726	-1.936

Notes:

(1) The bulge effective surface brightness of the artificial galaxy in mag arcsec^{-2}.

(2) The bulge effective radius of the artificial galaxy in arcsec.

(3) Fit results using the standard artificial image (see text) with $\mu_0 = 20$ R-mag arcsec^{-2} and $h = 20''$.

(4) As (3), but artificial image and fitting model have seeing of $2.5''$ instead of $1.5''$.

(5) As (3), but fitting model has $1.4''$ seeing instead of the $1.5''$ of the artificial image.

(6) As (3), but fitting model has $1.6''$ seeing instead of $1.5''$.

(7) As (3), but with sky level of the fitting model 1% too low compared to the real value in the artificial image.

(8) As (3), but with sky level of the fitting model 1% too high compared to the real value in the artificial image.

(9) As (3), but with $b/a = 0.65$ in fitting model and 0.75 in the artificial image.

(10) As (3), but with $b/a = 0.85$ in fitting model and 0.75 in the artificial image.

(11) As (3), with error of 20° in PA between image and model.

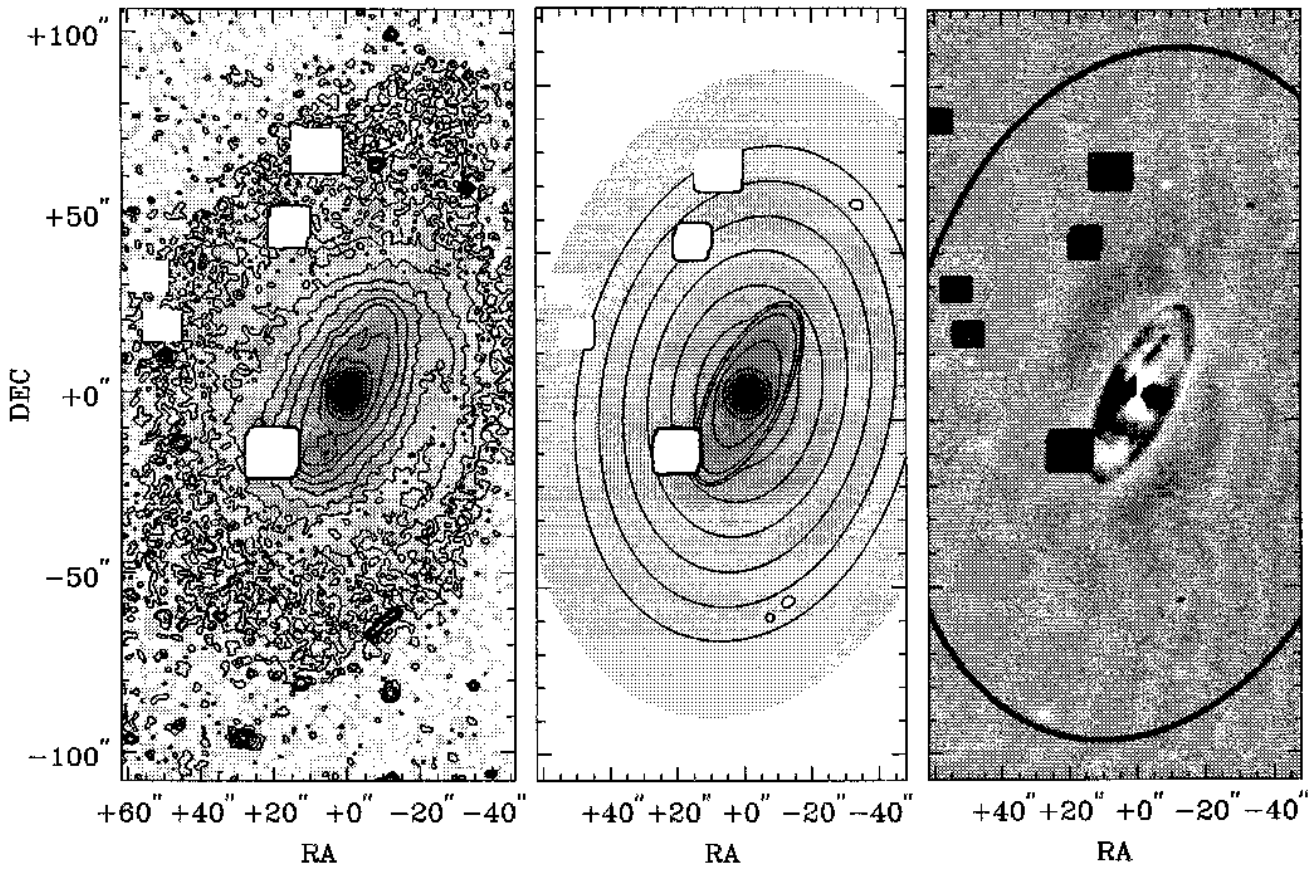

Fig. 1. Left: UGC 89 R passband image, with isophotes overlaid from 18 to 24 R-mag arcsec^{-2} in steps of 0.5 mag arcsec^{-2}. Center: Fitted model on the same grayscale and contour level as the left image. Right: Residual image using the 2D fit model of the center image. The ellipse indicates the area used for the fit and the b/a and PA of the fitted exponential disk. The fitted bar component shows up as the inner ellipse in the residuals. Structure in the bar region and the two arms coming off the ends of the bar are clearly visible and can not be fitted with this simple model

When the galaxy image showed a clear bar and when this bar resulted in an identifiable feature in the luminosity profile, a bar was added as a third component to the model. A Freeman bar (1966) was used, which is one of the few available analytic 2D descriptions for the luminosity of a bar

$$\Sigma_{\rm bar}(x,y) = \Sigma_{0,\rm bar}\sqrt{1-(x/a_{\rm bar})^2-(y/b_{\rm bar})^2}, \qquad (4)$$

where the free parameters are $\Sigma_{0,\rm bar}$, the bar central surface brightness, and $a_{\rm bar}$ and $b_{\rm bar}$, the semi major and minor axis of the bar respectively. Such a bar has elliptical isophotes and has its position angle ($\rm PA_{bar}$) as additional free parameter. No inclination dependent corrections were applied to the bar profiles, since the studied galaxies are not inclined very much.

Observations of galaxies are distorted by seeing. The model light distributions have to be corrected for this effect. Seeing is only important at the center of the galaxy where the light distribution strongly peaks. The disk and bar light distributions are far less peaked and generally do not dominate the center compared to the bulge, therefore only the bulge model profile was corrected for seeing.

To account for the seeing effects, the model profiles of the bulge were convolved with a Gaussian Point Spread Function (PSF) with the same dispersion (σ) as the Gaussians that were fitted to some field stars in the frame. For a radially symmetric light distribution around the center the seeing convolved profiles are described by

$$\Sigma_{\rm s}(r) = \sigma^{-2}{\rm e}^{-r^2/2\sigma^2}\int_0^\infty \Sigma(x)I_0(xr/\sigma^2){\rm e}^{x^2/2\sigma^2}\,x\,{\rm d}x, \qquad (5)$$

where $\Sigma(r)$ is the intrinsic surface brightness profile, σ the dispersion of the Gaussian PSF and I_0 the zero-order modified Bessel function of the first kind (Pritchet & Kline 1981).

The total model is simply the sum of the three components

$$\Sigma_{\rm tot}(x,y) = \Sigma_{\rm disk}(x,y) + \Sigma_{\rm bulge}(x,y) + \Sigma_{\rm bar}(x,y). \qquad (6)$$

Table 2. The test results of the 2D fit using an R passband image of UGC 438. Before the test a bulge with μ_e=18.954 R-mag arcsec^{-2} and r_e=2.5″ (the parameters resulting from the initial fit) was subtracted from the original image, leaving a bulgeless test image. The removed bulge was for the test replaced by an exponential bulge of the indicated model parameters (model μ_e, model r_e) and fitted by the 2D fit routine. The resulting fitted μ_0 and μ_e are in R-mag arcsec^{-2} and the h and r_e are in arcsec. NC indicates that no fit convergence was reached

model μ_e	model r_e = 2.5″				model r_e = 5.0″				model r_e = 1.25″			
	fitted μ_0	h	μ_e	r_e	μ_0	h	μ_e	r_e	μ_0	h	μ_e	r_e
16.454	18.891	12.91	16.453	2.502	19.025	13.42	16.457	5.054	18.869	12.81	16.373	1.192
17.207	18.891	12.91	17.205	2.502	19.026	13.42	17.213	5.087	18.869	12.81	17.037	1.125
18.201	18.891	12.91	18.201	2.502	19.026	13.42	18.216	5.205	18.870	12.81	17.719	0.923
18.954	18.891	12.91	18.954	2.502	19.025	13.42	18.977	5.406	18.873	12.83	17.792	0.638
19.707	18.891	12.91	19.703	2.485	19.020	13.40	19.735	5.725	18.882	12.87	17.359	0.353
20.459	18.888	12.90	20.415	2.401	18.997	13.31	20.454	6.011	NC			

3.3. *Fitting procedure*

To fit models to the data points a non-linear fitting algorithm capable of accepting different weights for each data point was applied. Non-linear fitting algorithms are particularly sensitive to the initial values provided, when searching for the minimum in the reduced χ^2 of the fit. If the initial values are not "reasonable", the fitting program can end up in a wrong local minimum. The results of the 1D decompositions described in Sect. 4 were used as initial values. The initial values for the bar were estimated by eye. The routine generally converged to the same result to within the formal errors, independent of the initial values. The formal fit errors were usually much smaller than the errors due to the uncertainties in the measurements and these errors will be discussed in detail in Sects. 4 and 5.

In decomposing 1D profiles it is common practice to fit in the logarithmic (magnitude) regime. This means that one is effectively trying to minimize the relative errors between model and data. Minimization in the logarithmic regime is not possible in the 2D case; because of the noise some pixels will have negative values (below sky level) in the outer parts of the galaxy image. To minimize relative errors in the linear regime, a difference between model and data in a low surface brightness region has to be given much more weight during the fitting than the same difference in a high surface brightness area. A weight function of the form $e^{r/h}$ was used, where h is the initial estimate of the disk scalelength and r is the inclination corrected distance of the pixel from the center. To reduce computing time all pixels outside 2.5 initial disk scalelengths were averaged over 5×5 pixels and given proportionally more weight.

The 2D fitting procedure consisted of several steps. First, all images of a galaxy obtained in different passbands were aligned, freed of foreground stars and their center was determined from the R passband image (see Paper I). This center was fixed while fitting the model components to the data. After the fitting routine had converged, the model light distribution was subtracted from the data. The points in the difference image that deviated more than 6 sigma (missed cosmic ray events and faint stars) were flagged and not used in the next iteration. This process was repeated twice, each time taking the initial estimates and the scalelength of the weight function from the results of the previous step. In general, the routine had already converged to a satisfactory result after the second step.

3.4. *Tests on artificial data*

The 2D fitting routine was extensively tested on artificial images to determine its reliability. Artificial images are not really representative of true galaxies, but can give an indication of the systematic effects due to measurement errors. By varying one by one the observables in the artificial images one can investigate which measurement error influences a model parameter the most.

The artificial images had the characteristics of a typical R passband observation: all artificial galaxies had an exponential disk with a μ_0 equal to 20 mag arcsec^{-2}, a scalelength of 20″ and axial ratio of 0.75. Just as with the typical observation the pixel size was set at 0.3″, the seeing at 1.5″ FWHM and the sky surface brightness at 20 mag arcsec^{-2} in the artificial images. An exponential bulge was added to each image, with the bulge parameters chosen from a range in effective surface brightness and radius . The images were created with photon and read out noise and a few areas were set to undefined values to mimic the removal of foreground stars. The initial fit estimates for the disk and bulge parameters were set at 10−30% off the intrinsic model values to check convergence. The final results showed very little sensitivity to the initial estimates.

The effect of different bulge-to-disk ratios was tested using the artificial images with the different bulge parameter values. The relative differences between artificial image input parameters and the model fit output parameters are listed in Table 1. The fitting routine reproduced the bulge and disk parameters to a very high degree of accuracy. The disk parameters were reproduced with less than 1.5% error. The bulge parameters were less well reproduced,

especially for very small effective radii and low effective surface brightnesses. These bulges are so small that they are unresolved with 1.5″ seeing in the small region where they are dominating over the disk surface brightness. For these extreme cases it is better to convolve not only the bulge model with the seeing, but also the disk. Increasing the seeing to 2.5″ in both the artificial image and the fitting model had no effect on the determination of the disk parameters and slightly decreased the fit performance for the bulge parameters, as can be seen in Table 1.

Some observables measured from the images (seeing, sky background level, b/a and PA) were used as fixed parameters in the fit models. To estimate their relative effects on the derived parameters, all artificial images were fitted again, but the fixed parameters in the fitting model were given a wrong value with respect to the true values in the artificial image. The typical maximum error was used for each of the fixed parameters. The test results can be found in Table 1. From these tests the largest error in μ_0 is expected to result from a wrong estimation of the sky background. The error will be of order 0.1 mag arcsec^{-2}, increasing, of course, for lower surface brightness galaxies. The errors in the scalelength are dominated by errors in sky brightness and b/a, and both result in errors less than 10% in the typical case. The errors in the bulge parameters are dominated by their brightness and scalelength relative to the disk parameters. The parameters of the brighter bulges are most effected by errors in the seeing. The effective radii of the lower surface brightness bulges are also influenced by sky brightness errors. Except for the extreme low surface brightness bulges and for bulges with effective radii smaller than 1″ the errors are never larger than 20%.

The fitting routine was also tested on some artificial images with a bar, but with eight free parameters only a limited parameter space could be explored. In general, the routine converged to satisfactory results in just a few iterations.

3.5. *Tests on UGC 438*

Clearly, artificial images are not a good representation of real galaxies. Therefore, the fitting routine was also tested for different bulge-to-disk ratios on an R passband image of UGC 438. A 2D fitted bulge was subtracted from the original image and replaced by artificial exponential bulges with a range in effective surface brightness and radius. The fit results for the different bulge parameters are listed in Table 2.

The fitting routine generally reproduces the parameters quite well. The disk parameters change little for the different bulges (μ_0 changes at most by 0.04 mag arcsec^{-2} and h by about 4%), but as with the tests on artificial images, the fitting routine breaks down for bulges with a small effective radius and a low surface brightness. Next to the explanations for this effect mentioned earlier for the artificial images, one has another problem when one tests on real images. The model bulge that was originally subtracted to create a bulgeless image might not be perfectly correct. One is then left with some residuals which have the greatest influence when later replaced by a low surface brightness bulge.

3.6. *Resulting parameters*

The results from the 2D fits for all galaxies in our sample are presented in Table 3 for the B and the K passband. This table contains observed data values. No corrections were applied for inclination and for internal and Galactic extinction. In 23 out of 86 cases it was found that the fits of at least the bulge improved if a bar was also included.

Figure 1 shows an example of an original, a model and a model subtracted image of UGC 89. The relative differences between model and data are quite small and the resulting difference image can be used to study small scale structures in the bulge and bar region and to study spiral arms. UGC 89 is a good example of a galaxy that can only be fitted correctly by a 2D method with a bar, as can be seen more clearly in the resulting 1D profile of Fig. 2.

In testing both artificial and real images it appears that the 2D fitting routine has difficulties fitting bulges with a low surface brightness and a small effective radius compared to the disk parameters. There are few galaxies in the sample with a fitted $r_e < 1$. This is only found in the B and V passbands when galaxies have Type II profiles. The routine fits a small bulge to these galaxy images to avoid filling up the "central hole" in the disk. The Type II behavior is always less pronounced at longer wavelengths and indeed in the K passband there are no galaxies with $r_e < 1$. Fortunately, there are no galaxies in the sample with a small effective radius *and* a low effective surface brightness of the bulge relative to the disk central surface brightness. Using these limitations in parameter space, the standard column in Table 1 indicates that the errors intrinsic to the fitting routine are expected to be less than 10%. The errors caused by other sources will be discussed in the next sections.

4. Comparison of different decomposition methods

The structural parameters derived in the previous section will be used in subsequent papers of this series. In order to assess the reliability of the derived relations in these papers, a good estimate of systematic and random errors in the fitted parameters has to be determined. The 2D fitting results will be compared to various conventional 1D methods to demonstrate the increased accuracy. The 1D methods will also be used to investigate the two most important sources of error in the bulge and disk parameters, namely the sky background error and the uncertainty in the shape of the bulge profile. The 2D method was too time consuming to be used for these tests.

Table 3. The results from the 2D fit model with μ_0, μ_e and $\mu_{0,bar}$ in mag arcsec^{-2}, h, r_e, a_{bar} and b_{bar} in arcsec and PA_{bar} in degrees. NP means a non-photometric observation, but the scale parameters are still determined

UGC	B								K							
	μ_0	h	μ_e	r_e	$\mu_{0,bar}$	a_{bar}	b_{bar}	PA_{bar}	μ_0	h	μ_e	r_e	$\mu_{0,bar}$	a_{bar}	b_{bar}	PA_{bar}
89	22.07	28.5	18.87	2.5	21.77	31.6	11.4	152.8	17.46	17.4	14.61	2.5	17.63	29.6	10.3	153.6
93	22.33	21.3	22.02	0.9	—	—	—	—	18.55	15.7	18.82	1.4	—	—	—	—
242	21.26	13.7	18.73	0.2	—	—	—	—	17.28	11.1	17.82	0.9	—	—	—	—
334	23.36	21.5	24.89	2.4	—	—	—	—	20.32	18.1	21.26	3.8	—	—	—	—
438	20.45	14.1	21.22	2.9	—	—	—	—	16.23	11.5	15.84	2.1	—	—	—	—
463	20.76	13.5	20.60	1.3	—	—	—	—	16.80	12.0	16.73	1.9	—	—	—	—
490	21.47	18.5	21.51	2.6	—	—	—	—	17.16	14.9	17.73	3.9	—	—	—	—
508	22.05	30.5	19.81	2.8	22.66	48.1	11.2	93.1	17.74	26.3	15.26	2.9	17.91	40.1	10.5	93.3
628	22.86	14.8	24.61	3.4	—	—	—	—	20.39	18.6	21.46	5.4	—	—	—	—
1305	22.02	33.9	21.24	3.8	—	—	—	—	17.61	26.5	17.00	4.2	—	—	—	—
1455	22.27	24.0	20.47	2.1	22.15	13.2	4.9	19.6	17.64	16.2	15.67	2.0	18.06	16.5	6.2	22.5
1551	22.47	25.8	24.81	2.6	—	—	—	—	18.98	24.4	20.06	2.9	—	—	—	—
1559	22.48	20.0	23.42	3.8	—	—	—	—	20.08	19.6	20.21	5.8	—	—	—	—
1577	22.44	22.1	20.89	2.2	22.80	32.9	10.8	144.5	18.26	17.6	16.01	1.8	18.42	26.8	8.9	145.1
1719	22.45	21.7	20.99	1.6	22.88	13.3	5.2	127.6	17.73	14.3	16.68	1.9	18.45	15.9	5.2	129.3
1792	21.65	17.1	21.31	1.3	—	—	—	—	17.48	14.4	17.21	1.8	—	—	—	—
2064	22.28	20.1	20.78	0.8	—	—	—	—	18.01	17.6	16.25	1.1	—	—	—	—
2081	22.31	19.1	23.46	1.4	—	—	—	—	19.44	19.4	19.83	2.5	—	—	—	—
2124	22.34	23.0	20.07	2.7	21.96	21.4	7.0	100.1	18.11	21.3	15.89	2.7	17.62	21.3	6.1	100.2
2125	23.20	26.8	21.01	1.7	23.47	34.6	6.9	79.5	—	—	—	—	—	—	—	—
2197	22.57	18.2	23.43	2.1	—	—	—	—	17.97	12.3	18.60	2.1	—	—	—	—
2368	23.67	28.3	19.82	1.3	22.50	52.9	14.0	156.9	18.88	18.1	15.19	1.7	18.41	48.0	11.9	156.9
2595	—	—	—	—	—	—	—	—	—	—	—	—	—	—	—	—
3066	22.03	14.6	21.40	0.4	—	—	—	—	17.09	11.2	17.25	1.6	—	—	—	—
3080	21.99	17.2	19.88	0.2	—	—	—	—	18.21	15.1	18.79	1.7	—	—	—	—
3140	20.90	13.1	20.46	2.0	—	—	—	—	16.96	11.3	15.99	2.1	—	—	—	—
4126	21.83	22.6	20.01	1.4	23.34	45.7	9.6	38.1	18.02	18.7	16.09	1.8	19.01	35.2	10.8	48.5
4256	21.18	17.6	19.22	0.7	—	—	—	—	17.27	15.8	16.15	2.1	—	—	—	—
4308	21.34	20.0	19.78	0.8	—	—	—	—	17.66	16.4	17.06	1.9	—	—	—	—
4368	21.52	17.6	22.52	2.0	—	—	—	—	17.81	14.7	18.89	2.2	—	—	—	—
4375	21.31	20.2	22.18	2.1	—	—	—	—	17.21	16.9	18.46	2.5	—	—	—	—
4422	22.04	31.0	20.92	3.5	—	—	—	—	18.38	27.0	16.55	3.4	—	—	—	—
4458	21.72	19.8	19.50	3.0	—	—	—	—	17.75	17.9	15.05	2.5	—	—	—	—
5103	20.50	17.8	19.84	1.3	—	—	—	—	16.56	14.5	16.07	1.9	—	—	—	—
5303	21.32	36.8	21.41	3.0	—	—	—	—	17.89	37.7	17.72	4.3	—	—	—	—
5510	20.66	20.4	19.22	1.3	—	—	—	—	17.37	18.4	16.53	2.2	—	—	—	—
5554	20.98	19.1	19.31	1.5	—	—	—	—	16.94	16.7	15.66	2.1	—	—	—	—
5633	23.13	27.8	23.67	0.9	22.99	23.5	3.0	161.5	20.01	29.4	21.03	1.5	19.88	23.2	3.7	162.5
5842	21.44	30.3	21.01	0.9	—	—	—	—	18.01	27.4	18.52	2.2	—	—	—	—
6028	20.49	15.3	21.57	0.5	—	—	—	—	17.27	13.0	18.66	1.6	—	—	—	—
6077	20.88	18.4	20.17	1.1	—	—	—	—	17.49	18.4	17.22	2.1	—	—	—	—
6123	NP	27.1	NP	2.1	—	—	—	—	17.29	25.0	15.46	2.0	—	—	—	—
6277	20.88	27.9	18.98	1.3	—	—	—	—	17.25	21.5	16.54	2.9	—	—	—	—
6445	20.55	16.1	20.19	2.6	20.94	11.6	4.1	157.6	16.83	14.0	16.17	2.6	17.11	11.4	4.5	154.4
6453	20.91	21.3	22.04	7.9	—	—	—	—	17.16	16.3	17.87	5.6	—	—	—	—
6460	20.66	27.6	19.63	1.8	—	—	—	—	17.15	24.1	16.53	2.1	—	—	—	—
6536	NP	21.7	NP	1.9	NP	13.5	9.3	9.0	18.57	20.3	15.47	1.9	17.80	12.7	8.1	16.5
6693	21.60	18.9	21.72	0.7	—	—	—	—	17.99	16.7	17.13	1.3	—	—	—	—
6746	21.38	17.7	20.18	2.2	—	—	—	—	17.30	16.0	15.64	2.1	—	—	—	—
6754	22.71	32.0	21.58	4.2	—	—	—	—	18.32	21.7	15.77	1.8	—	—	—	—
7169	20.11	13.2	20.20	1.7	—	—	—	—	16.55	10.0	16.38	2.3	—	—	—	—
7315	19.99	14.8	20.75	1.5	—	—	—	—	16.03	14.6	16.96	2.1	—	—	—	—
7450	21.17	64.9	20.14	7.8	—	—	—	—	17.30	48.5	15.72	6.3	—	—	—	—
7523	21.49	36.0	19.61	4.0	22.10	47.2	11.8	144.5	17.70	32.5	15.11	3.1	17.87	44.1	12.9	143.6
7594	21.03	52.4	19.16	3.6	21.72	50.2	21.5	11.8	16.94	44.8	15.21	4.1	17.73	51.2	19.6	8.7

Table 3. continued

UGC	B								K							
	μ_0	h	μ_e	r_e	$\mu_{0,bar}$	a_{bar}	b_{bar}	PA_{bar}	μ_0	h	μ_e	r_e	$\mu_{0,bar}$	a_{bar}	b_{bar}	PA_{bar}
7876	NP	21.2	NP	1.7	—	—	—	—	18.55	22.1	20.06	4.4	—	—	—	—
7901	20.07	25.1	20.06	3.0	—	—	—	—	16.06	19.7	16.22	3.8	—	—	—	—
8279	20.52	13.6	22.87	7.0	—	—	—	—	16.90	11.5	18.59	5.9	—	—	—	—
8289	21.80	33.2	19.59	3.2	—	—	—	—	17.90	21.1	15.84	3.2	—	—	—	—
8865	21.89	32.0	20.10	2.7	21.83	19.8	9.4	169.2	18.27	29.3	15.65	2.3	17.84	27.2	9.5	168.4
9024	24.08	28.2	21.64	2.1	—	—	—	—	22.07	45.4	19.15	3.6	—	—	—	—
9061	22.63	62.0	20.08	2.1	21.97	15.0	6.5	111.3	18.75	39.3	16.22	2.8	17.73	16.8	4.0	110.2
9481	21.22	17.6	21.36	1.1	22.87	27.0	4.3	94.2	18.03	17.5	17.26	1.6	18.46	21.5	6.2	98.7
9915	NP	17.7	NP	2.6	—	—	—	—	17.21	15.7	16.58	2.3	—	—	—	—
9926	20.13	17.9	20.16	3.1	—	—	—	—	16.45	16.6	15.96	4.3	—	—	—	—
9943	20.40	20.0	20.92	2.7	21.37	19.8	6.2	73.3	16.60	17.6	16.55	2.3	17.16	19.7	5.9	70.3
10083	21.51	23.3	22.65	4.3	22.08	44.8	8.8	149.2	17.60	18.9	18.64	4.2	18.50	44.2	10.1	149.3
10437	24.03	33.6	23.28	8.9	—	—	—	—	NP	17.0	NP	7.1	—	—	—	—
10445	21.76	20.3	22.99	2.3	—	—	—	—	19.00	19.6	20.08	4.5	—	—	—	—
10584	21.77	23.8	21.22	1.7	—	—	—	—	18.18	19.4	17.47	2.2	—	—	—	—
11628	22.27	38.8	20.10	3.1	—	—	—	—	17.19	21.9	15.09	2.6	—	—	—	—
11708	21.51	17.9	21.77	1.9	—	—	—	—	NP	14.4	NP	2.0	—	—	—	—
11872	20.46	18.3	20.68	7.0	20.61	13.2	3.7	17.6	15.71	12.6	14.94	2.5	16.01	12.8	6.0	13.3
12151	23.27	26.1	24.78	6.4	—	—	—	—	20.14	21.7	21.19	4.8	—	—	—	—
12343	21.95	50.7	21.32	4.3	22.01	66.9	11.0	7.0	17.67	39.7	15.94	3.4	17.67	68.2	12.6	10.7
12379	21.99	19.3	20.40	2.1	—	—	—	—	17.44	15.7	15.33	1.9	—	—	—	—
12391	21.50	15.7	18.03	0.2	—	—	—	—	17.79	13.8	17.36	1.2	—	—	—	—
12511	22.46	24.4	22.38	1.6	—	—	—	—	18.35	13.2	18.09	2.1	—	—	—	—
12614	20.94	21.6	18.76	0.7	—	—	—	—	17.24	20.2	15.00	1.2	—	—	—	—
12638	22.17	21.4	21.74	1.3	—	—	—	—	18.27	19.8	18.24	2.6	—	—	—	—
12654	21.76	19.6	22.73	2.0	—	—	—	—	17.98	15.2	18.82	3.0	—	—	—	—
12732	23.66	29.8	25.30	11.0	—	—	—	—	NP	37.5	NP	10.5	—	—	—	—
12754	21.81	52.7	22.21	5.2	21.83	48.1	6.7	98.0	NP	49.2	NP	7.6	NP	44.6	8.3	100.6
12776	23.39	61.3	20.01	2.0	22.02	22.6	8.9	171.5	19.30	30.2	15.52	2.0	17.90	21.0	7.9	171.6
12808	20.31	13.8	17.50	0.7	—	—	—	—	—	—	—	—	—	—	—	—
12845	22.69	24.6	23.32	2.4	—	—	—	—	NP	18.1	NP	2.5	—	—	—	—

4.1. *One-dimensional decompositions*

One-dimensional decomposition methods are well known in the literature (Kormendy 1977; Schombert & Bothun 1987; Simien 1989; Capaccioli & Caon 1992; Andredakis & Sanders 1994) and will be described briefly. The resulting parameters are only available in electronic form.

The most elementary way to obtain the disk parameters, the "marking the disk method", was also used by Freeman (1970), when he found the disk central surface brightness to be constant among galaxies. The linear part of the luminosity profile, plotted on a magnitude scale, was marked and a linear least squares fit was made to the data points in the indicated range. To be able to compare the disk parameters of a galaxy in different passbands, I used the same range in radii for all passbands. The resulting parameters can be quite sensitive to the minimum and maximum radius chosen to fit. The difficulties of the "marking the disk" method have been discussed by Giovanelli et al. (1994) and results obtained by different authors were compared by Knapen & van der Kruit (1991), showing remarkable differences. These differences were mainly caused by a change in scalelength at a lower surface brightness.

The "marking the disk" method yields disk parameters that are intuitively correct for the human eye. However, the luminosity profile is a combination of bulge and disk light and to get correct results both should be fitted simultaneously (Kormendy 1977). The numerical method to decompose the luminosity profiles used here is essentially identical to the method described by Andredakis & Sanders (1994). A non-linear χ^2 minimalization routine was used to fit the model profiles to the data points in the logarithmic regime. Both bulge and disk model profiles were convolved with the seeing PSF using Eq. (5) and the fits were limited by the same maximum radii used for the "marking the disk" fit.

As already indicated in Sect. 1, several different radial luminosity laws have been proposed for the light of bulges. One of the more general forms for the light profile of the bulge is the generalized exponential law, originally

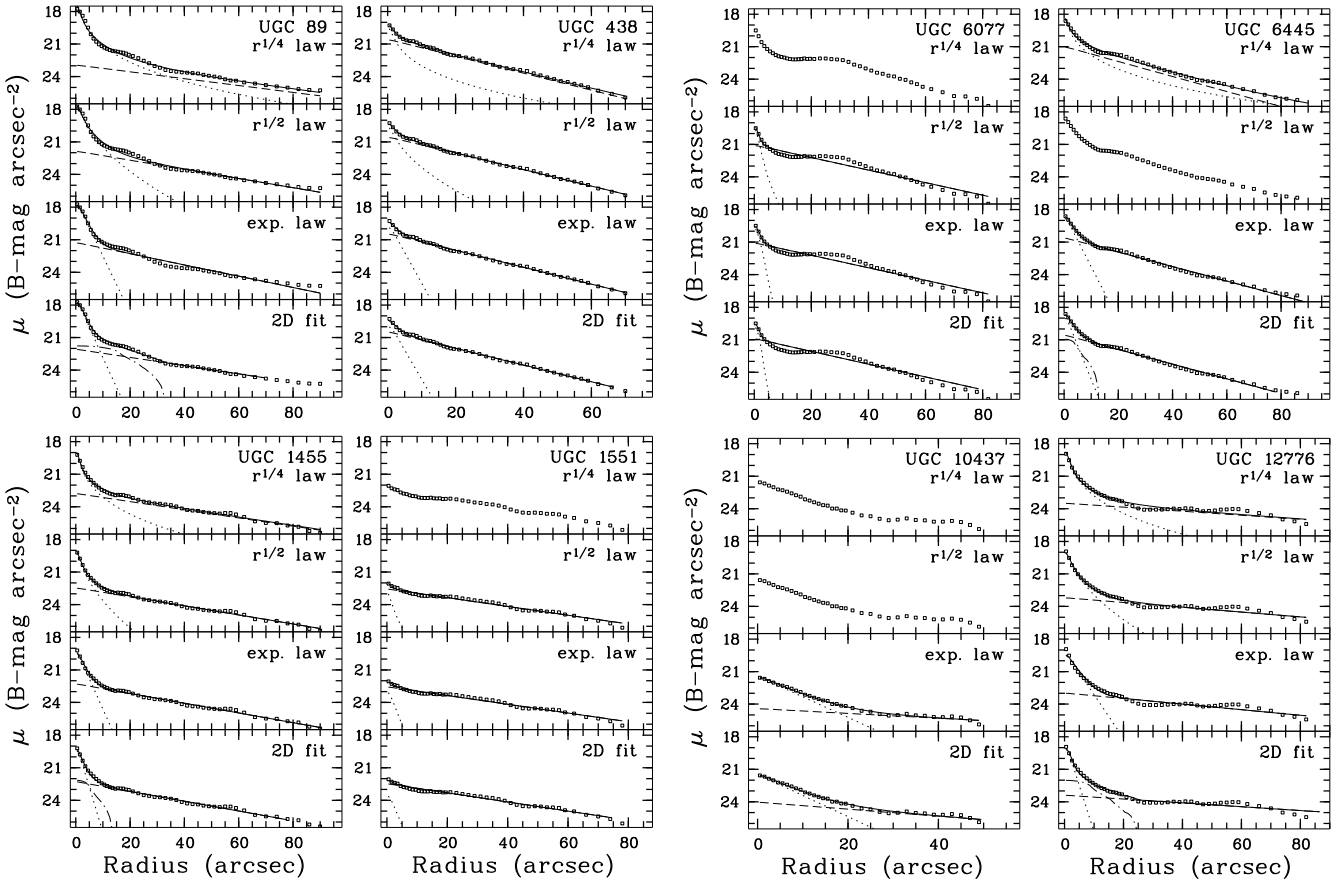

Fig. 2. Some examples of the fits made to the B passband surface brightness profiles. The squares indicate the measured profile, the dashed line represents the fitted disk, the dotted line the fitted bulge and the dashed-dotted line the bar. The full line is the sum of the different model components. The method to extract the model luminosity profiles from the 2D model images was the same as used on the real data

proposed by Sérsic (1968):

$$\Sigma(r) = \Sigma_0 \mathrm{e}^{-(r/h)^{1/n}}. \quad (7)$$

This generalized exponential law has been applied to fit elliptical and S0 galaxies by Caon et al. (1993) and to dwarf ellipticals by Young & Currie (1994).

As a first step, the fitting of an exponential disk and a generalized exponential bulge profile was tried. A wide variety of initial values for the five free parameters were tried, but for most of the galaxies the fits did not converge to physically acceptable values (negative Σ_0, Σ_e, h or r_e). The value of n in Eq. (7) was of order 0.5–5 in the cases where the fit did converge, that is for the galaxies with pronounced bulges. For most galaxies the bulge light dominates over the disk light at only a few data points and these few points do not carry enough information to limit the shape parameter n.

To reach more stable results the same fits were made again with n fixed to values 1, 2 and 4. With $n=4$ and after redefining Σ_0 and h into effective parameters, Eq. (7) translates in the most commonly used bulge fitting function, the de Vaucouleurs (1948) or $r^{1/4}$ law:

$$\Sigma(r) = \Sigma_\mathrm{e} \mathrm{e}^{-7.67(r/{r_\mathrm{e}}^{1/4}-1)}. \quad (8)$$

Setting $n = 2$ in Eq. (7) gives an "$r^{1/2}$ law" profile:

$$\Sigma(r) = \Sigma_\mathrm{e} \mathrm{e}^{-3.672(r/{r_\mathrm{e}}^{1/2}-1)}. \quad (9)$$

In the case of $n = 1$ in Eq. (7) one has the exponential law normally used for disk profiles, which translates into Eq. (3) when rewritten to effective parameters and which was also used for the 2D fit.

More stable results were reached than with the general exponential law, but the intrinsic properties of the $r^{1/4}$ law still made it impossible to reach convergence in many cases. With $n=2$ the situation improved considerably and using an exponential profile for the bulge, the fitting converged for all galaxies except for UGC 6028. This galaxy has a very small bulge in a Type II profile (Freeman 1970) and therefore the fitting routine tends to make the bulge negative in order to create a hole in the disk profile. The

fits with the exponential bulge are the most stable; convergence is reached more often and the fit results are less sensitive to initial values with the exponential bulge than with the other tested profiles. The tests on the artificial images in Sect. 3.4 showed that one of the main sources of error in the bulge and disk parameters was the uncertainty in the sky background level. The maximum errors in the fit parameters due to this uncertainty were calculated for each galaxy using the sky errors determined in Paper I. All 1D fits were repeated with the maximum sky error estimate added to and subtracted from the luminosity profile. These error estimates will be used in the next sections.

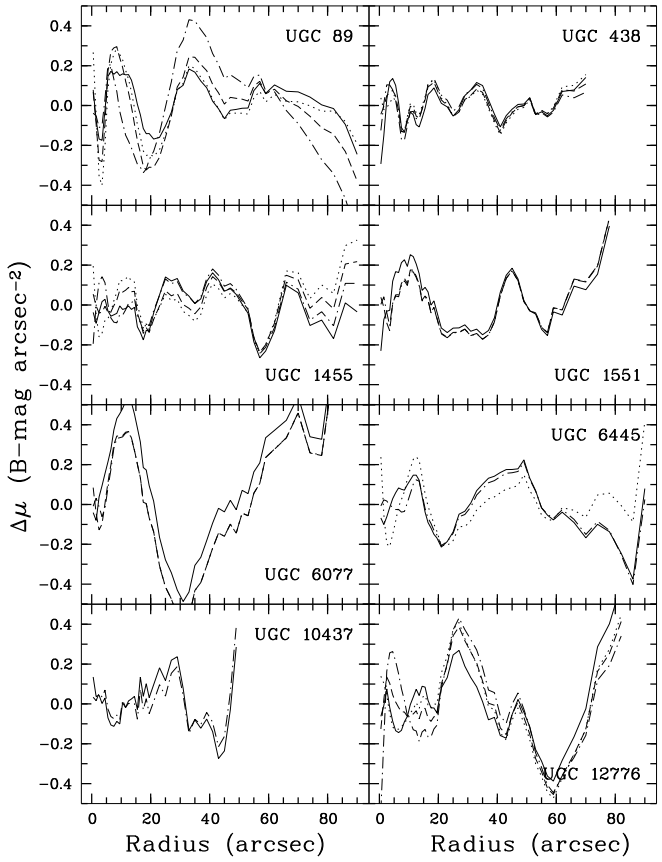

Fig. 3. The residuals $\Delta\mu$ between data and model for the galaxies plotted in Fig. 2. The dotted line indicates the model with the $r^{1/4}$ law bulge, the dashed line the $r^{1/2}$ law bulge fit, the dashed dotted line the exponential bulge fit and the full drawn line the 2D fit method. Note that generally the 2D fit method results in smaller residuals, but that the difference between the models is small compared to the intrinsic fluctuations in the luminosity profile

4.2. *Profile comparison*

The different decompositions of eight galaxies are discussed in more detail as it will give some insight in the problems dealing with bulge/disk decompositions. Figure 2 shows some typical best and worst cases of four different decomposition models on B passband profiles/images. Images of these galaxies can be found in Paper I.

UGC 89 is probably the clearest example in the sample of a galaxy with three distinct components, which can only be fitted correctly using a 2D fitting technique. In Fig. 2 we see that in the $r^{1/4}$ law fit the bulge fills up the bar region, but also replaces part of the disk. The central surface brightness of the disk is probably too faint and the scalelength too large in this fit. When we use an $r^{1/2}$ or an exponential bulge, the disk tries to fill up the bar region, making the fit to the outer exponential part of the profile worse. The disk parameters are obviously incorrect for these fits, but now the surface brightness is too faint and the scalelength too small. Only including a bar yields a satisfying result, also displayed in Fig. 1.

UGC 438 is a galaxy with a small bulge and a distinct exponential disk with some enhanced star formation in the spiral arms near the center. All fitting methods seem to be equally justified, but notice the very extended bulge in the case of the $r^{1/4}$ bulge profile.

UGC 1455 is a symmetrical galaxy with a small bar/oval component in the center. All fits seem equally justifiable as long as we assume that the oval component is part of the bulge. The μ_0 becomes gradually fainter going from $r^{1/4}$ to the exponential bulge. If we assume that the bar is part of the disk, which is likely as some spiral arms start at the ends of the bar, the 2D fit is the best fit.

UGC 1551 has a low surface brightness disk with some flocculent star formation and a very small bulge. The $r^{1/4}$ profile did not converge for the B passband (though it did for the other passbands). Even though convergence was reached with the other fitting functions, the bulge results can hardly be called reliable; the small bulge is very hard to fit.

UGC 6077 is a typical case of a Type II profile, where the exponential outer profile does not continue all the way inward before the bulge takes over the luminosity in the central part of the galaxy. Morphologically these galaxies are in general barred with strong spiral arms forming at the end which are tightly wound to form a ring. Sometimes the bar is less pronounced. Moving to longer wavelengths the bump becomes less pronounced as the enhanced star formation does not show up so clearly at those wavelengths. None of the tested fitting models is able to decompose this type of galaxies well. One has to adjust the exponential law of the disk to contain an inner hole or one has to model spiral arms in the disk. None of the fitting techniques are correct (the $r^{1/4}$ law fit did not even converge for this galaxy) and the central surface brightnesses and scalelengths

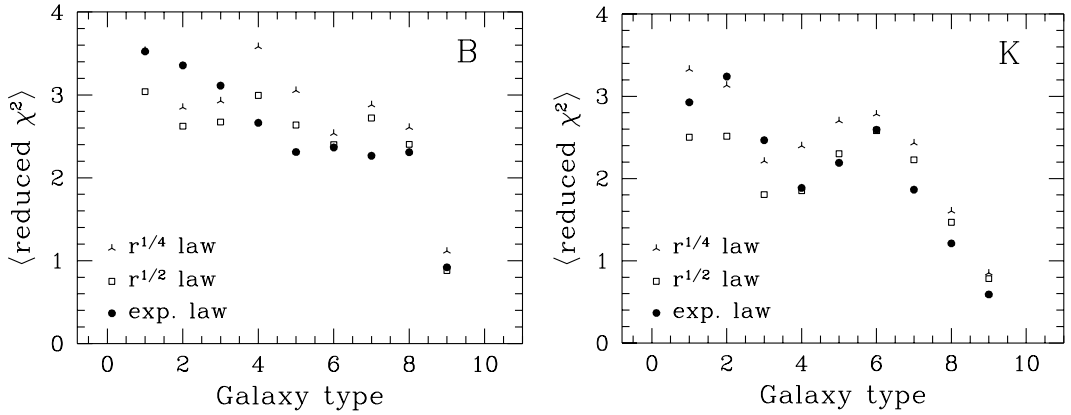

Fig. 4. The average reduced χ^2 values per morphological type for the 1D fit with different bulge models

found are just an indication of the extent and surface brightness of the disk.

UGC 6445 a galaxy with a small oval component, has a less pronounced Type II profile. Because of a slight shift in steepness of the luminosity profile in the outer region of the galaxy, the $r^{1/4}$ fit will tend to dominate in the central and outer region. Consequently bulge and disk are equally important over the whole extent of the galaxy in such a fit. Inclusion of a bar or oval component immediately diminishes the bulge contribution at large radii, even if one would fit an $r^{1/4}$ bulge profile. Clearly the 2D fit is the best option for this galaxy.

UGC 10437 is an example of one of the galaxies in the sample with a very low surface brightness disk. The fits made to this kind of galaxy are in general very unstable as the disk disappears rapidly in the sky noise. This means that the profile that can be fitted only extends over a few scalelengths. The H and K passband observations especially could pose some problems as these showed hardly anything else other than the bulge above the sky noise (see also UGC 334, UGC 628 and UGC 9024). The fits with $r^{1/4}$ and $r^{1/2}$ bulge profiles only converged to unphysical values for this galaxy, the exponential 1D bulge and the 2D fit yield nearly the same result, as might be expected for a nearly face-on galaxy.

UGC 12776 is a galaxy that consists mainly of a bar, with two arms originating at the ends. Similar galaxies are UGC 2368 and UGC 10083. Obviously a bar should be included in the models to fit these galaxies, but we have to keep in mind that in these cases the bar really seems to belong to the disk. The central surface brightness of such a galaxy is probably best described by the sum of the contributions of the disk and the bar.

Figure 3 shows the residuals between models and data. This figure shows that including a bar in the fitting routine can indeed improve the overall fit, but also shows

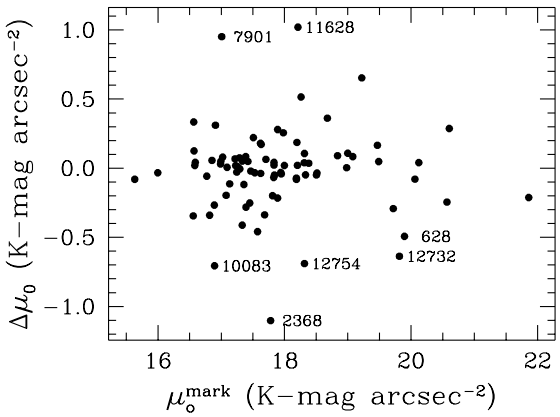

Fig. 5. The difference between the central surface brightnesses obtained with the "marking the disk" method and the 2D fit method ($\Delta\mu_0 = \mu_0^{\rm mark} - \mu_0^{\rm 2D}$) as function of μ_0 in the K passband. The UGC numbers of the most deviant galaxies are indicated

that the residuals are dominated by fluctuations in the profiles. These fluctuations are not due to signal-to-noise problems, but are intrinsic to the light distribution of the galaxy. This makes it difficult to decide which bulge model is best, as the change in reduced χ^2 is small compared to the reduced χ^2 value itself. One would need additional components to fit the fluctuations, but this is beyond the scope of this work.

4.3. *Comparison of χ^2 values*

An exponential bulge was used in the 2D fitting technique, which was motivated by the 1D test results. One such test is the comparison of the reduced χ^2 values for the different bulge models. Figure 4 shows the different reduced χ^2 values as function of morphological type. Note that the χ^2 values are smaller in the K passband than in the B passband and that the differences between the χ^2 values

Table 4. The median of the fit parameter errors for all galaxies, where the maximum error in the sky background subtraction was used to calculate the uncertainty in the fit parameters. The errors in μ_0 and μ_e are in mag arcsec^{-2}, the relative errors in h and r_e were defined by $\Delta h/h$ and $\Delta r_e/r_e$

Band	median error in μ_0				median error in h				median error in μ_e			median error in r_e		
	marking	$r^{1/4}$	$r^{1/2}$	exp.	marking	$r^{1/4}$	$r^{1/2}$	exp.	$r^{1/4}$	$r^{1/2}$	exp.	$r^{1/4}$	$r^{1/2}$	exp.
B	0.02	0.07	0.06	0.05	0.037	0.044	0.033	0.029	0.15	0.06	0.02	0.50	0.26	0.14
V	0.03	0.08	0.07	0.05	0.033	0.035	0.030	0.025	0.18	0.06	0.02	0.33	0.21	0.12
R	0.02	0.07	0.06	0.04	0.027	0.034	0.026	0.023	0.11	0.05	0.02	0.40	0.18	0.09
I	0.03	0.11	0.10	0.07	0.042	0.030	0.026	0.021	0.18	0.08	0.03	0.43	0.15	0.08
H	0.04	0.16	0.20	0.12	0.041	0.039	0.028	0.023	0.28	0.12	0.04	0.43	0.15	0.09
K	0.04	0.17	0.14	0.11	0.049	0.032	0.025	0.021	0.27	0.09	0.04	0.39	0.16	0.09

Table 5. The mean relative change in disk parameters due to different techniques for all galaxies where the fit routine converged to physical values for all techniques. All mean changes are relative to the "marking the disk" method, with $\Delta\mu_0$ in mag arcsec^{-2}, $d = 2(h_{\rm mark} - h_{\rm other})/(h_{\rm mark} + h_{\rm other})$ dimensionless. The errors are standard deviations

Band		$\langle\Delta\mu_0\rangle$				$\langle d\rangle$			
	#	$r^{1/4}$ law	$r^{1/2}$ law	exp. law	2D fit	$r^{1/4}$ law	$r^{1/2}$ law	exp. law	2D fit
B	71	–0.21 ± 0.31	–0.06 ± 0.20	0.06 ± 0.20	0.07 ± 0.24	–0.01 ± 0.14	0.02 ± 0.10	0.06 ± 0.11	0.06 ± 0.14
V	64	–0.21 ± 0.28	–0.16 ± 0.53	0.03 ± 0.18	0.02 ± 0.31	0.02 ± 0.12	–0.00 ± 0.09	0.04 ± 0.09	0.03 ± 0.13
R	72	–0.25 ± 0.37	–0.13 ± 0.38	0.05 ± 0.21	0.02 ± 0.30	–0.01 ± 0.15	–0.01 ± 0.12	0.04 ± 0.11	0.03 ± 0.12
I	68	–0.28 ± 0.39	–0.21 ± 0.50	0.04 ± 0.19	0.03 ± 0.29	0.01 ± 0.15	–0.03 ± 0.15	0.03 ± 0.10	0.03 ± 0.12
H	34	–0.19 ± 0.47	–0.17 ± 0.35	–0.00 ± 0.43	–0.04 ± 0.56	0.05 ± 0.22	0.00 ± 0.15	0.00 ± 0.09	-0.02 ± 0.13
K	65	–0.22 ± 0.40	–0.15 ± 0.45	0.08 ± 0.19	0.02 ± 0.28	0.02 ± 0.18	0.00 ± 0.09	0.05 ± 0.09	0.02 ± 0.10

of the different bulge models are small compared to these χ^2 values themselves.

For galaxies with types later than Sb, the fits with the exponential bulge give the smallest residuals. For galaxies in the range from Sa-Sb, the $r^{1/2}$ law bulge fits give the best results. In this range, the $r^{1/4}$ law and exponential law bulge give comparable results in reduced χ^2 values. Therefore one could propose an intermediate transition type bulge for early spirals between the $r^{1/4}$ law ellipticals and the exponential bulges of late-type spirals. This could be analogous to the pure elliptical systems, where low luminosity systems are less centrally concentrated than high luminosity systems (Young & Curie 1994).

The results of the study by Andredakis & Sanders (1994) are confirmed using this sample. Exponential bulges are statistically at least as justified as $r^{1/4}$ law bulges. When the galaxy image does not contain enough information to determine the shape of the bulge, the exponential bulge is preferred for galaxies with classification later than Sb. For early-type spiral galaxies an $r^{1/2}$ law bulge is a good alternative. For consistency reasons, only the results obtained with the exponential bulge will be used in subsequent papers when analyzing this large sample of galaxies.

4.4. *Comparisons of errors due to sky uncertainties*

The tests on artificial images discussed in Sect. 3 indicated that the uncertainty in the sky background level is, once a bulge model has been chosen, the largest source of error. As explained before, the maximum errors due to incorrect sky background subtraction were only calculated for the 1D methods. The median relative errors for each parameter and each method are listed in Table 4. Two trends can be seen in this table:
1) the median errors in the surface brightness parameters increase going from the *B* to the *K* passband, while the uncertainties in the scale parameters decrease and
2) the median errors in *all* parameters decrease moving from the fits with the more centrally peaked $r^{1/4}$ law bulge profile to the fits with the shallower exponential bulge profile.

A change in sky background level affects mostly the faint outer regions of the galaxy profiles. The $r^{1/4}$ law profile offers often a greater contribution to the outer parts of galaxies than the exponential bulge profile and will be more affected by a sky level change. The parameters resulting from the fit with the exponential bulge are the most stable and reproducible according to the results in Table 4 which is independent of the conclusion whether this bulge model is correct or not.

4.5. *Comparison of the resulting disk parameters*

As a final point in the comparison of the different bulge models and fitting methods the resulting parameters are compared. Table 5 lists the average differences in the disk parameters using the different methods. The disk parameters of all different models are compared to those of the "marking the disk" method. The change in central surface

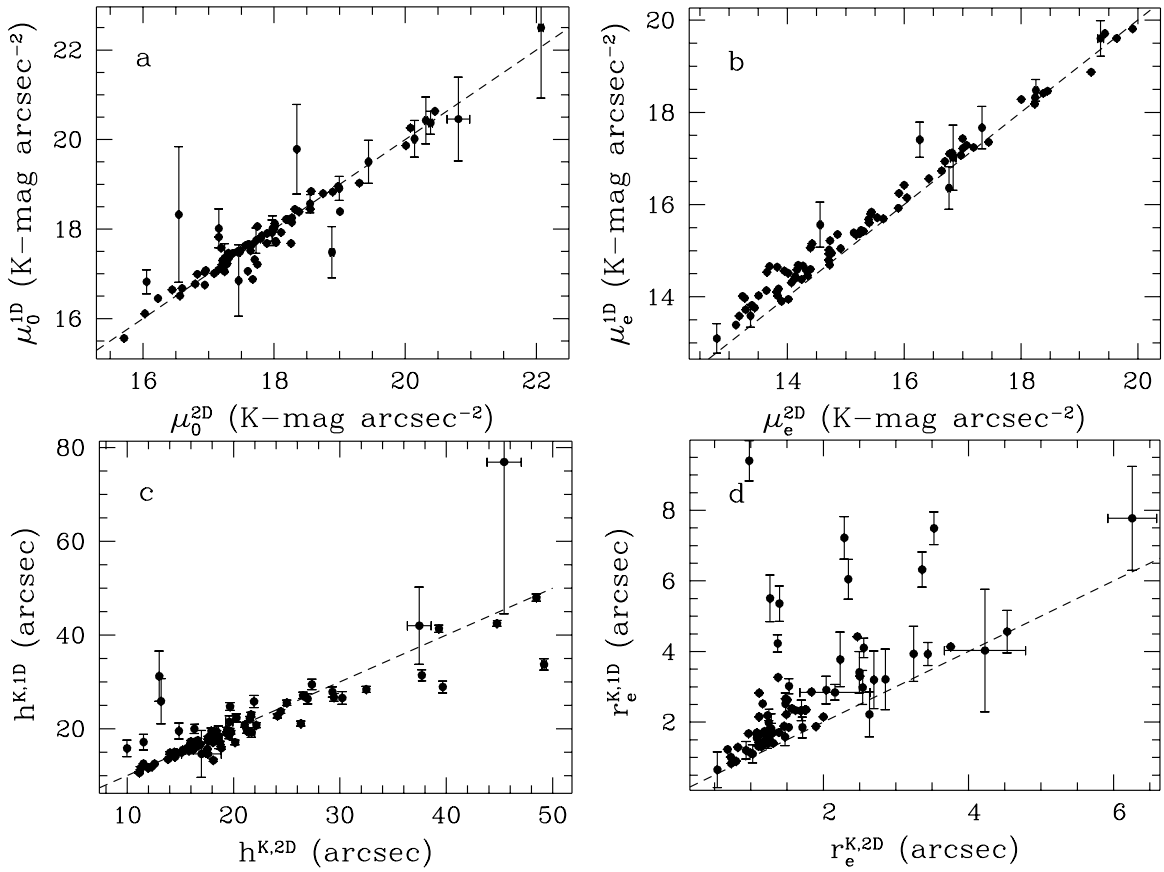

Fig. 6. A comparison between the K passband parameters obtained with the 1D and the 2D methods. An exponential bulge profile was used for both the 1D and the 2D method. **a**) Central surface brightness of the disk, **b**) effective surface brightness of the bulge, **c**) scalelength of the disk and **d**) effective radius of the bulge. The errors in the 2D parameters are the formal fit errors of the fit routine, the errors in the 1D parameters are the maximum errors due to the uncertainty in the sky background subtraction

brightness $\Delta\mu_0 = \mu_{0,\rm mark} - \mu_{0,\rm other}$ is on average the largest for the $r^{1/4}$ law bulge and small for the exponential bulge in both the 1D and 2D case. The central surface brightness of the disk is lower for the $r^{1/2}$ and $r^{1/4}$ law bulges as part of the disk light is replaced by the light of these more extended bulges. The average relative change in scalelength ($d = 2(h_{\rm mark} - h_{\rm other})/(h_{\rm mark} + h_{\rm other})$) is a few percent at most for all models. The scalelengths become on average a little bit smaller. The standard deviations of the differences in μ_0 are much larger for the $r^{1/2}$ and $r^{1/4}$ law bulges than for the exponential bulges. Apparently the methods using exponential bulges yield more often disk parameters that are in accordance with the "marking the disk" results, which represent the human intuition.

A comparison the results from the "marking the disk" fit with the 2D fit (Fig. 5), shows that the central surface brightnesses agree for most galaxies to within 0.5 mag arcsec^{-2}. The few exceptions to this can be easily explained. On the one hand, the surface brightness is fainter in the 2D case for UGC 2368, UGC 10083 and UGC 12754, as a bar is making up a large fraction of the disk and for some low surface brightness galaxies (UGC 628 and UGC 12732), because the distinction between the nearly absent bulge and the disk is hard to make. On the other hand, UGC 7901 and UGC 11628 have a gradual change in slope of their luminosity profile, which is interpreted differently by the 2D fitting program than by the human eye. The 2D fit central surface brightnesses are much brighter.

Figure 6 shows a comparison between the 1D and 2D bulge and disk parameters, both obtained with the exponential bulge profile. The errorbars on the 2D results indicate the formal fitting errors of the fitting routine, thus the uncertainty in the χ^2 minimum found by the routine. The errors in the 1D parameters result from recalculations of the fit with the sky background uncertainties added and subtracted.

Two points can readily be made from these errors: 1) the errors due to sky uncertainties are almost always much larger than the formal fitting errors and 2) the data points which are the most deviant from the equality line have in general also the largest uncertainty due to the sky errors.

The errors due to sky uncertainty are apparently also indicators of the differences between both fitting methods.

The 1D and 2D disk parameters in Fig. 6 agree quite well without any systematic deviations. The effective surface brightness of the bulge shows a small but systematic deviation, the surface brightnesses determined with the 1D method are most of the times a little fainter. The comparison of the effective radii shows the largest deviations. The 2D effective radii are smaller, especially for the galaxies where a bar was fitted. The profile comparisons of Fig. 2 showed that these smaller effective radii are more realistic.

4.6. *The exponential bulge versus other bulge models*

The exponential bulge profile was used in the 2D fitting technique instead of the more widely used $r^{1/4}$ law profile. The previous tests have shown that this is justified. The profile decompositions look at least as good as with other bulge models, which is reflected in the reduced χ^2 results. Table 4 shows that the exponential bulge results are least effected by the uncertainty in the sky level and Table 5 shows that the exponential bulge fit reflects the "marking the disk" results the most. The choice for the exponential bulge is obvious if one further realizes that the exponential bulge fit, contrary to the other models, almost always converges without fine tuning the initial parameters. One could propose to use $r^{1/2}$ law bulges for early-type spiral galaxies, but for consistency reasons I will use only the exponential bulge law results in subsequent papers.

5. Error discussion

Good error estimates of the fit parameters are important to determine the reliability of the derived relations in the next papers of this series. All sources of error and the typical percentage of error they cause in the different bulge and disk parameters are discussed.

In the decomposition methods discussed in this article one is confronted with three kinds of uncertainties: 1) uncertainties in the component profiles, 2) the uncertainties due to the fitting method and 3) measurement errors. The first two items give systematic effects in the derived parameters, but make comparisons within such a framework still possible. The last item has no systematic effect, assuming measurement errors are randomly distributed. Each of these points will be addressed separately, indicating the order of magnitude uncertainty in the resulting parameters.

1) Errors due to uncertainties in component profiles

- The best choice for the description of the bulge light is probably the generalized exponential (Eq. (7)), as it includes both the $r^{1/4}$ and the exponential law. Its mathematical peculiarities make it here less useful in combination with an exponential disk profile. Therefore the exponential function for the bulge is preferred, as it gives a first moment analysis of the part of the bulge that is seen above the disk luminosity. In this way, a surface brightness and a scale size of the central region of the bulge can be determined. These quantities must have some physical meaning, even though they show only a weak relation to the ones obtained with $r^{1/2}$ and $r^{1/4}$ law bulges. The average value of μ_0 of the disk will be 0.2 mag arcsec^{-2} fainter using these bulges and the rms differences will increase to 0.4 mag arcsec^{-2} with respect to the "marking the disk" fit. The scalelengths of the disks are about the same for all bulge models used. The uncertainty in the disk parameters for a typical galaxy in this data set is larger due to bulge profile uncertainty than due to sky background uncertainty (compare results in Table 4 and standard deviations in Table 5).
- The use of exponential light profiles for disks of spiral galaxies is well established, but Type II profiles introduce an uncertainty. Are we dealing with a hole in the light distribution (intrinsic or due to dust) or do we have an extra stellar component at intermediate radii in the form of a ring of spiral arms? Morphology and color considerations favor the second option. Therefore one has to include the inner region in the fit as this is also part of the disk and observe at wavelengths which are least affected by young stellar populations. In the B passband, the Type II profiles can give uncertainties of order 20% in the disk parameters and up to 50% in the bulge parameters. In the K passband the effect is strongly reduced to order 10% for all parameters.

2) Uncertainties induced by different fitting methods

- The uncertainties in the "marking the disk" method have been discussed by Giovanelli et al. (1994) and by Knapen & van der Kruit (1991). They showed that the uncertainties using this method are of order 15%. It has been argued that this method gives *systematically* wrong results (Kormendy 1977; Phillipps & Disney 1983; Davies 1990) which will be discussed in Paper III (de Jong 1996).
- The decomposition of the 1D profile in a bulge and a disk component should in principle be better than the previous method, but when performed with an exponential bulge profile the disk parameters hardly change compared to the "marking the disk" results. Byun (1992) showed that this method gives systematically wrong results for inclined galaxies.
- The 2D fitting method is intrinsically the best method tested here. It includes the effect of inclination and makes it possible to introduce a non-axisymmetric component in the form of a bar. With respect to the double exponential 1D fit it has little effect on the disk parameters and on μ_e of the bulge. The estimate of r_e of the bulge improves. The tests on artificial images showed that the errors in the parameters are at most a few percent for bulges with r_e larger than $1''$.

– One source of error that has never been investigated in detail is the choice of weighting function for the fitting routine. I have only used weighting schemes which reduce relative errors between model and data, but one could argue that the inner part of galaxies should get more weight as the signal-to-noise is better in these regions. Likewise one could also argue that the outer part of the luminosity profile should get more weight as many more points are sampled (this is what happens automatically in the 2D fitting technique). Therefore even a single model for bulge and disk luminosity distribution has an intrinsic uncertainty depending on where one puts the most weight for the fitting accuracy. It is hard to define an acceptable range of weighting functions, but the uncertainty in the disk parameters induced in this way is estimated to be at most 5% for most galaxies. It will be of order 10% for the bulge parameters.

3) Uncertainties caused by measurement errors

– The dominant source of error in both bulge and disk parameters is the uncertainty in the sky background subtraction. As a second order effect b/a is also important for the estimate of μ_0. The seeing estimate influences the determination of the parameters of relatively small bulges. Each of these errors has at most order 10% effect on the disk parameters and a 20% effect on the bulge parameters. The errors will be slightly larger for low surface brightness galaxies, due to the relatively larger contribution of the sky background error.
– Another source of error, independent of the fitting method employed, stems from the determination of the zero-point of the magnitude scale. In Paper I, we calculated that this was for our sample in the range from 0.03 to 0.12 mag arcsec^{-2}, resulting in this contribution being of the same order of or less than the above mentioned measurement errors.

6. Conclusions

The bulge, disk and bar parameters of the 86 spiral galaxies presented in Paper I were calculated. In the different decomposition methods that were explored, we were confronted with three kinds of uncertainties: 1) the uncertainties in the component profiles, 2) the uncertainties due to the fitting method and 3) measurement errors. The first two items will give systematic effects in the derived parameters, but comparisons within such a framework are still possible. The last item has no systematic effect, assuming measurement errors are randomly distributed.

In conclusion, the use of the 2D fitting technique with exponential light profiles for both bulge and disk yields the most reproducible and representative component parameters. Assuming that the 2D model with exponential profiles for both bulge and disk is a reasonable correct description of the global structure of a galaxy, the estimated maximum errors of the structural parameters are of order 20%. These errors are dominated by the uncertainty in the sky background level. The errors in the disk parameters will double if the model for the bulge is better represented by an $r^{1/4}$ law profile. The errors on the bulge parameters will then be very uncertain. The determined parameters will be used in the subsequent articles in these series.

The two dimensional decomposition technique exploited here has many advantages above other often used decomposition techniques. Still we are far away from full scale 3D models which link complete self-consistent dynamics of the different components to a 2D morphological projection.

Acknowledgements. I would like to thank Yanis Andredakis, Piet van der Kruit, Reynier Peletier and David Sprayberry for the fruitful discussions. Erwin de Blok, Joyce Majewski, René Oudmaijer and Arpad Szomoru are thanked for their many useful suggestions on the manuscript. I would like to thank the anonymous referee for the useful comments that helped to improve the manuscript. This research was supported under grant No. 782-373-044 from the Netherlands Foundation for Research in Astronomy (ASTRON), which receives its funds from the Netherlands Foundation for Scientific Research (NWO).

References

Andredakis Y.C., Sanders R.H., 1994, MNRAS 267, 283
Block D.L., Wainscoat R.J., 1991, Nat 353, 48
Burstein D., 1979, ApJ 234, 829
Byun Y.-I., 1992, Ph.D. Thesis, The Australian National University
Capaccioli M., Caon N., 1992, In: Longo G., Capaccioli M., Busarello G. (eds.) Morphological and Physical Classification of Galaxies. Kluwer, Dordrecht, p. 99
Capaccioli M., Held E.V., Nieto J.-L., 1987, AJ 94, 1519
Caon N., Capaccioli M., D'Onofrio M., 1993, MNRAS 265, 1013
Davies J.I., 1990, MNRAS 244, 8
de Jong R.S., 1996, A&A, (in press) (Paper III)
de Jong R.S., van der Kruit P.C., 1994, A&AS 106, 451 (Paper I)
de Vaucouleurs G., 1948, Ann. d'Astrophys. 11, 247
de Vaucouleurs G., 1959, Hdb. d. Physik 53, 311
de Vaucouleurs G., de Vaucouleurs A., Corwin H.G., Buta R.J., et al., 1991, Third Reference Catalog of Bright Galaxies. Springer-Verlag, New York (RC3)
D'Onofrio M., Capaccioli M., Caon N., 1994, MNRAS 271, 523
Frankston M., Schild R., 1976, AJ 81, 500
Freeman K.C., 1966, MNRAS 133, 47
Freeman K.C., 1970, ApJ 160, 811
Giovanelli R., Haynes M.P., Salzer J.J., Wegner G., Da Costa L.N., Freudling W., 1994, AJ 107, 2036
Hubble E.P., 1930, ApJ 71, 231
Jaffe W., 1983, MNRAS 202, 995
Jensen E.B., Thuan T.X., 1979, in: Photometry, Kinematics and Dynamics of Galaxies, Univ. of Texas, Austin
Kent S.M., 1986, ApJS 91, 1301

Kent S.M., Dame T., Fazio G., 1991, ApJ 378, 131
King I.R., 1966, AJ 71, 64
Knapen J.H., Kruit P.C., van der, 1991, A&A 248, 57
Kormendy J., 1977, ApJ 217, 406
Kormendy J., 1993, in: Dejonghe H., Habing H.J. (eds.) IAU Symp. 153, Galactic Bulges. Kluwer, Dordrecht, p. 209
Kormendy J., Bruzual A., 1978, ApJ 223, L63
Kormendy J., Illingworth G., 1982, ApJ 256, 460
Nilson P., 1973, Uppsala General Catalog of Galaxies, Roy. Soc. Sci., Uppsala (UGC)
Phillipps S., Disney M.J., 1983, MNRAS 203, 55
Pritchet C., Kline M.I., 1981, AJ 86, 1859
Schombert J.M., Bothun G.D., 1987, AJ 93, 60
Scorza C., Bender R., 1990, A&A 235, 49
Sérsic J.-L., 1968, Atlas de galaxias australes, Observatorio Astronomica, Cordoba
Shaw M.A., Gilmore G., 1989, MNRAS 237, 903
Simien F., 1989, in: Corwin H.G., Bottinelli L. (eds.) The World of Galaxies. Springer-Verlag, New York, p. 293
Simien F., Michard R., 1990, A&A 227, 11
van der Kruit P.C., 1979, A&AS 38, 15
Wainscoat R.J., Freeman K.C., Hyland A.R., 1989, ApJ 337, 163
Young C.K., Currie M.J., 1994, MNRAS 268, L11